Supplementary Information to

Secondary Aerosol Formation in Incense Burning Particles by Ozonolysis and Photochemical Oxidation via Single Particle Mixing State Analysis

Zhancong Liang[1,2], Liyuan Zhou[1,2], Xinyue Li[1], Rosemarie Ann Infante Cuevas[1,2], Rongzhi Tang[1,2], Mei Li[3,4], Chunlei Cheng[3,4], Yangxi Chu[5], Patrick. K.H. Lee[1], Alvin. C.K. Lai[1], Chak K. Chan[1,2,6]*

[1] School of Energy and Environment, City University of Hong Kong, Hong Kong, China

[2] City University of Hong Kong Shenzhen Research Institute, Shenzhen, China

[3] Institute of Mass Spectrometry and Atmospheric Environment, Guangdong Provincial Engineering Research Center for On-line Source Apportionment System of Air Pollution, Jinan University, Guangzhou 510632, China

[4] Guangdong-Hongkong-Macau Joint Laboratory of Collaborative Innovation for Environmental Quality, Guangzhou 510632, China

[5] State Key Laboratory of Environmental Criteria and Risk Assessment, Chinese Research Academy of Environmental Sciences, Beijing, 100012, China

[6] Low-Carbon and Climate Impact Research Centre, City University of Hong Kong, Hong Kong, China

*To whom the correspondence should be addressed: *chak.k.chan@cityu.edu.hk*

Content

Figure S20. The NF of new organic peaks in aged particles.

Table S1. The classification of particles and RPA of total nitrate peaks of aged particles at different laser fluences.

Table S2. Potential peaks from the inorganics and elemental carbons.

Text S1. Estimation of the OH exposure.

SO_2 was used to calculate the OH exposure in the Go:PAM. The UVC lamps were turned on to warm up for ~30 min and turned off. Then, O_3 (300, 800, 1500 ppb) and SO_2 (~200 ppb) were introduced to the Go:PAM with the UVC lamps turned off until its initial concentration remained constant at steady-state conditions, which typically took around 5 min. The $[SO_2]$ was recorded as $[SO_2]_{Initial}$. After that, the UVC lamps were turned on until the final $[SO_2]$ stabilized and was recorded as $[SO_2]_{Final}$. The time scale for the stabilization of $[SO_2]$ was around 4 min. The OH exposure at each condition is calculated using Eq. (A1):

$$OH\ exposure = \frac{1}{k_{OH,SO_2}} \times -ln\left(\frac{[SO_2]Final}{[SO_2]Initial}\right) \quad \text{(A1)}$$

where $k_{OH,SO2} = 9 \times 10^{-13}$ cm^3 molec^{-1} is the bimolecular rate constant between OH and SO_2 (Davis et al., 1979). The equation above is the result of integrating the differential rate equation for SO_2 and assuming pseudo-first order kinetics. The estimation of external OH reactivity (i.e., the OH reactivity with VOCs) requires VOC analysis and is not available in our study. Therefore, the OH exposure shown in this study may have been underestimated.

Text S2. Estimation of the mass hygroscopic growth factor (GF) by AIOMFAC model.

Based on the AIOMFAC model (Zuend et al., 2008), we obtained the weight fraction *w* of water and solutes (i.e., dry particles) in KNO_3 and KCl particles, respectively. Then, the GF is estimated as equation A2:

$$GF = \frac{m_{wet}}{m_{dry}} = \frac{m_{dry} + m_{water}}{m_{dry}} = 1 + \frac{m_{water}}{m_{dry}} = 1 + \frac{w_{water}}{w_{dry}} \quad \text{(A2)}$$

where m_{wet}, m_{dry} and m_{water} are the mass of wet particle, dry particle, and particulate water at different relative humidity (RH), respectively. The GF of KNO_3 and KCl particles as a function of time is shown in Figure S18. We did not consider efflorescence in the figure since the efflorescence RH for the KNO_3 and KCl are around 50%, much lower than 80% used in this study.

Text S2. The evolution of organic fragments.

We only showed NF ratios larger than 1 to focus on SOA formation. The positive spectra of both O_3-Dark-aged and O_3-UV-aged particles show NF increases for +30[NO] or [CH_2NH_2] (possibly due to nitrates, oxidized NOC, or amine), +44[CO_2] or [N_2O] (oxidized organics), +53[C_4H_5] and +69[C_5H_9] (aromatic hydrocarbons) (Wang et al., 2009; Silva et al., 2000; Dall'osto et al., 2013) (Figure S19). The negative spectra show increases for -137[$C_8H_9O_2$] (possibly methyl guaiacol) (Pagels et al., 2013; Gaie-Levrel et al., 2012) and -57[C_2HO_2] (a glyoxylate fragment) (Sullivan et al., 2007; Cheng et al., 2017), as well as -16[O]. O_3-UV-aged particles showed 200-folds and 10-folds NF increases for -137[$C_8H_9O_2$] and -57[C_2HO_2], respectively, significantly greater than that for UV-aged particles (~2-folds). Compared to OH chemistry, the UV photoactivity of compounds in particulates contributes minorly to organic chemistry (Figure S19).

Figure S20 show the NF of the new peaks in aged particles, which cannot (Dall'osto et al., 2009) be shown in the NF ratio plot due to their absence in fresh particles (zero denominator). O_3-Dark-aged particles show NF decreases of m/z +186 to +189 (probably PAHs) (Dall'osto et al., 2009) with increasing [O_3]. In contrast, O_3-UV-aged particles show NF increases of -31[CH_3O] or [HON], +123[$C_7H_7O_2$] and +124[$C_7H_8O_2$] (probably guaiacol) (Diab et al., 2015), and m/z +140 (probably HULIS) (Qin et al., 2006) with increasing OH exposure. These apparent changes in NF of organics fragments indicate the oxidative evolution of organics and likely formation of SOA, although the molecular characterization was hindered by severe fragmentation.

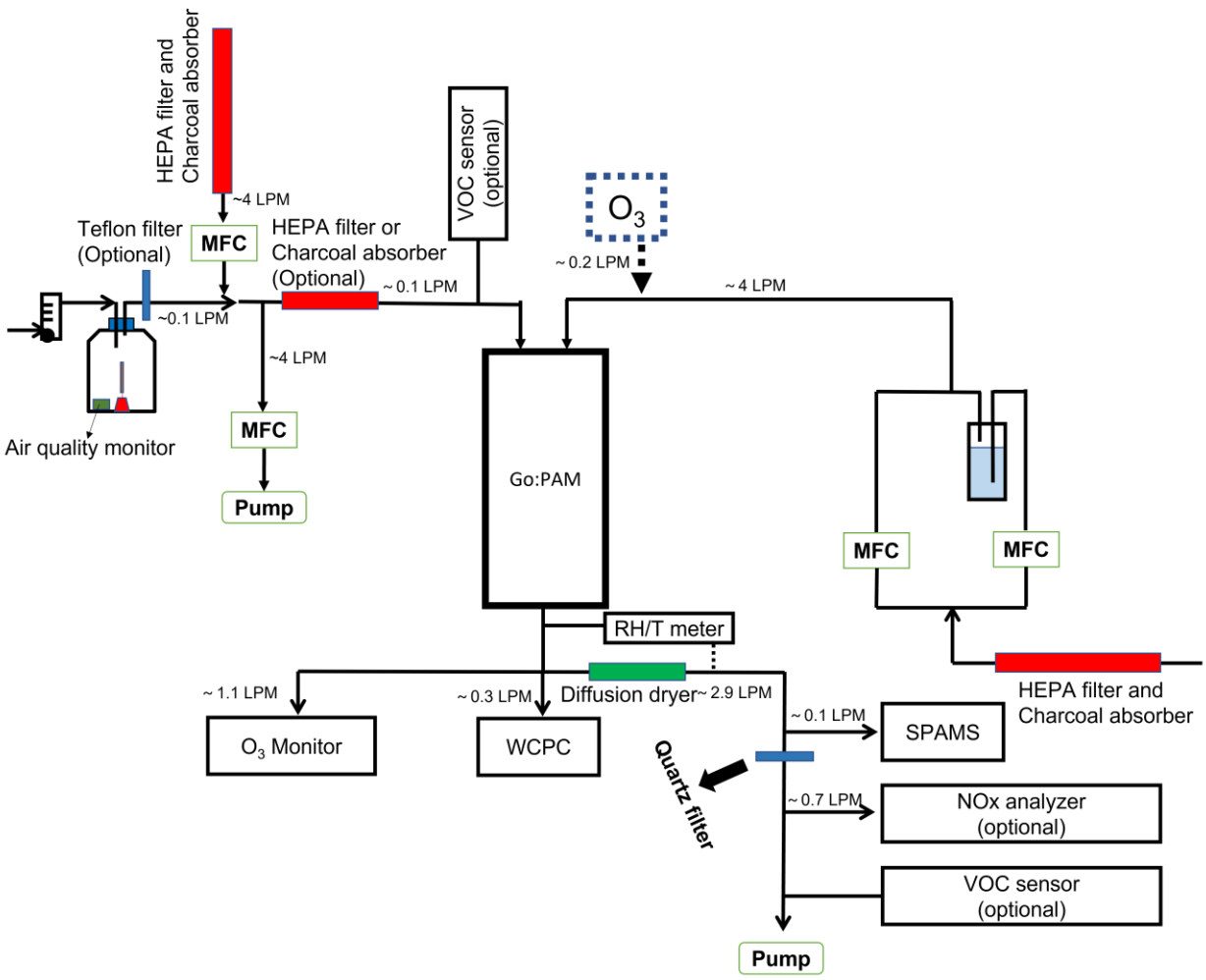

Figure S1. The schematic of the experimental set-up. The NOx analyzer and the VOC sensor were used only in the experiment for determining the gas removal efficiency and NOx decay under OH exposure.

Figure S2. The appearance of the incense sticks.

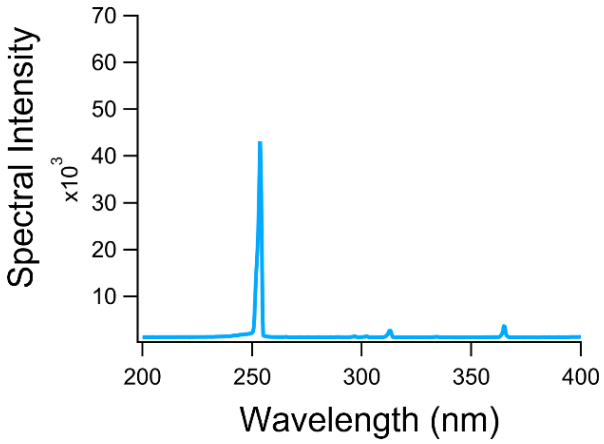

Figure S3. The emission spectrum of the UVC lamps.

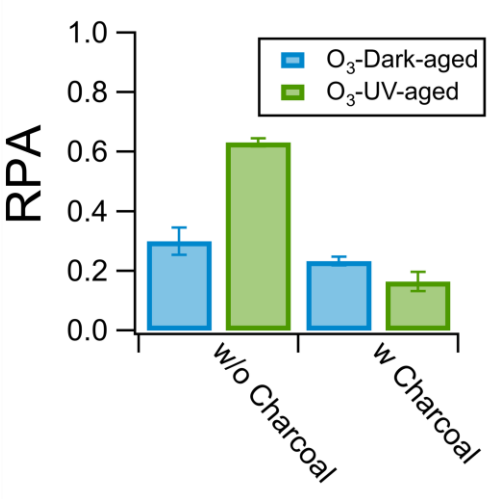

Figure S4. RPA of summed nitrate peaks of aged incense burning particles in the presence and absence of charcoal absorber.

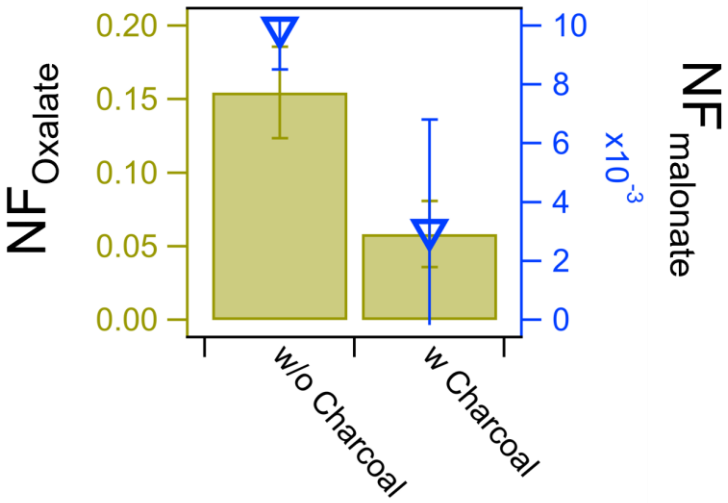

Figure S5. NF of oxalate and malonate of O_3-UV-aged incense burning particles (1500ppb O_3 + UV) in the presence and absence of a charcoal absorber.

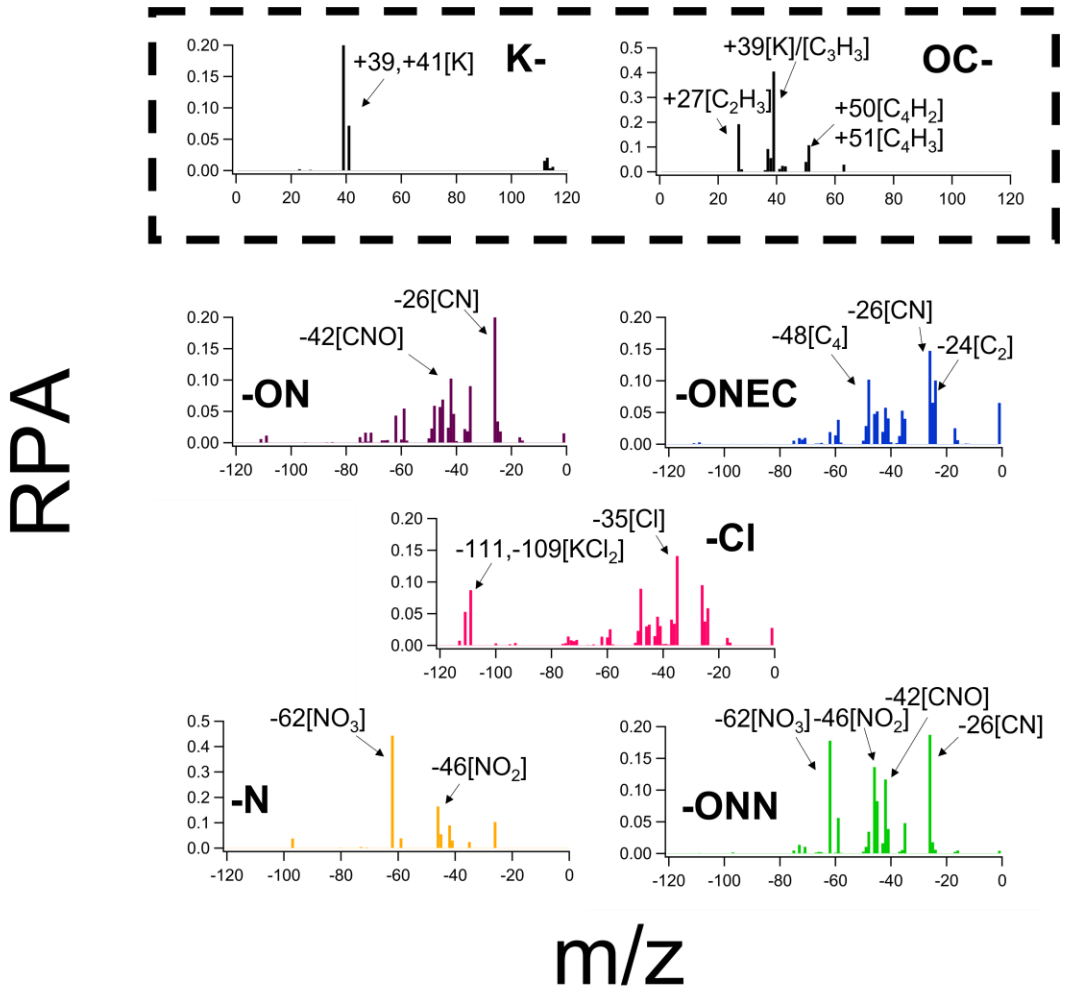

Figure S6. Positive (K- and OC-) and negative spectra (-ON, -ONEC, -Cl, -N, and -ONN) of different categorizations of particles. The spectral characteristics of these categories are similar under different conditions.

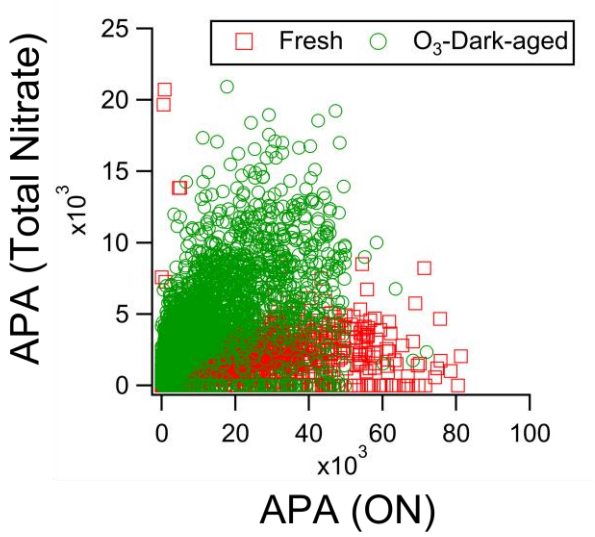

Figure S7. APA of ON as a function of APA of total nitrate in fresh and O_3-Dark-aged particles.

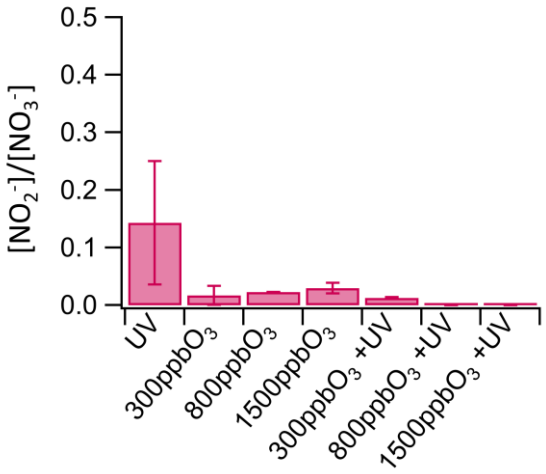

Figure S8. $[NO_2^-]/[NO_3^-]$ in water-extract of aged particles. Noted that the NO_2^- in 800ppb O_3+UV and 1500ppb O_3+UV experiments are undetectable.

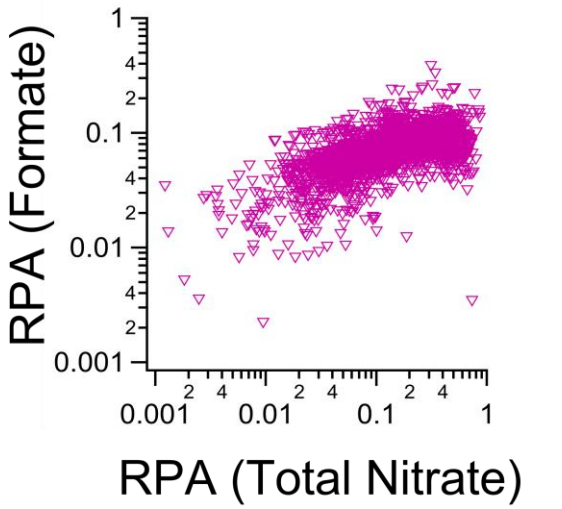

Figure S9. RPA of total nitrate as a function of RPA of formate.

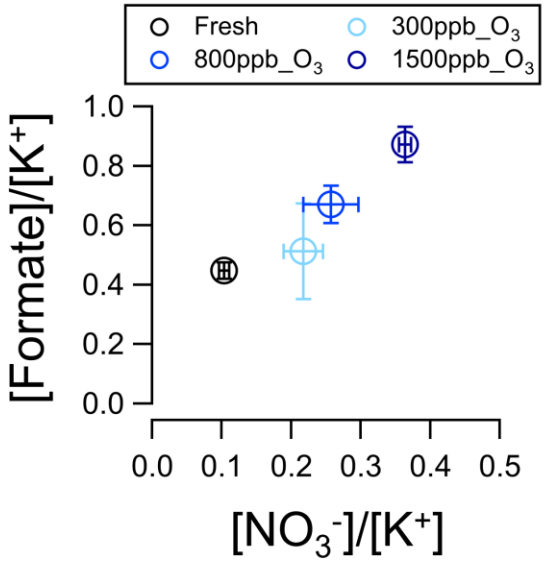

Figure S10. [Formate]/[K^+] as a function of [NO_3^-]/[K^+] in the water-extract of fresh and O_3-Dark-aged incense burning particles.

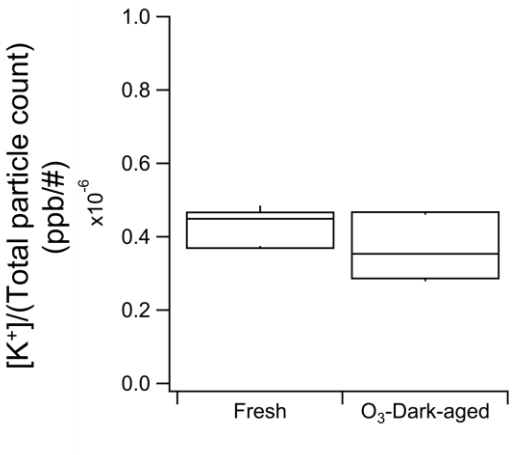

Figure S11. The whisker-box plot of the [K^+] in the particle water-extract measured by IC normalized by the total counts of collected particles for IC measurement. The error bar shows one standard deviation. We assume there was no new particle formation under ozone exposure since the WCPC showed comparable particle number concentration in the presence and absence of ozone.

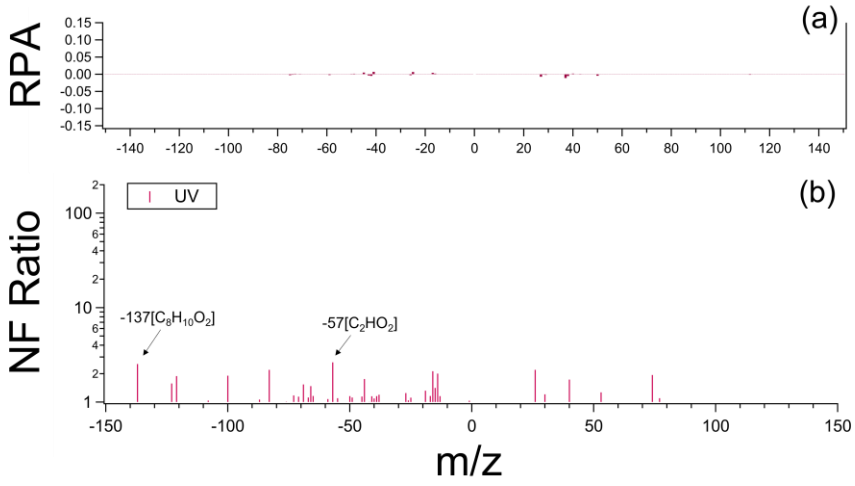

Figure S12. (a) The difference (aged minus fresh) of the average organic spectra of UV-aged particles; (b) The NF ratio (aged to fresh) of UV-aged particles to fresh particles, as a function of m/z [-150, 150].

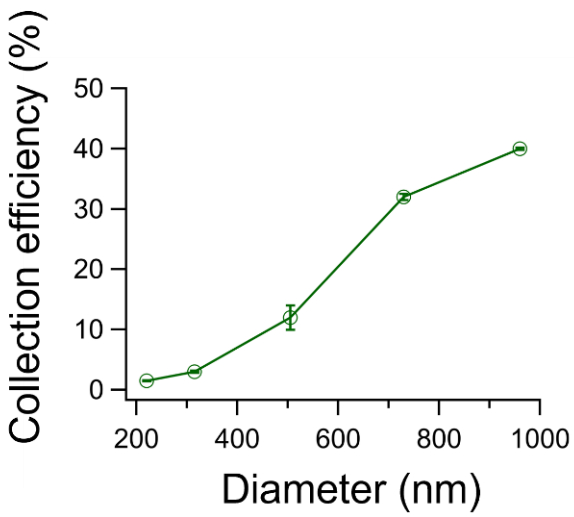

Figure S13. Relation between the particle collection efficiency of Polystyrene Latex particles and diameter in SPAMS.

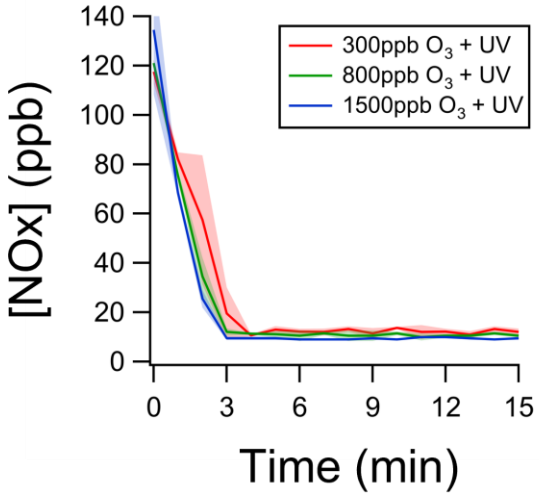

Figure S14. Evolution of [NOx] under different OH exposure as a function of time. The shadings show one standard deviation. The [NOx] was equilibrated without O_3 and UV at 0 min.

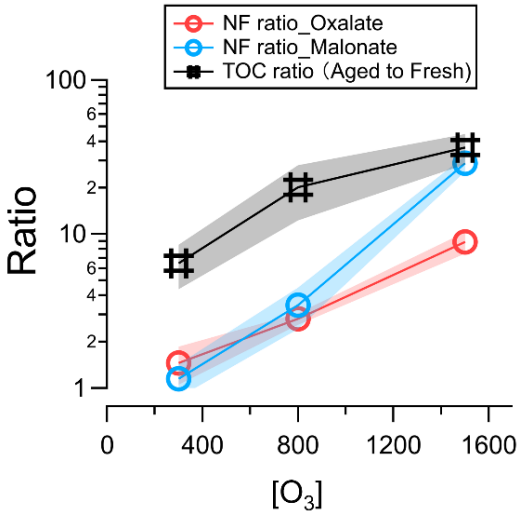

Figure S15. The NF ratios (aged to fresh) of oxalate and malonate, and TOC ratios as a function of [O_3] in O_3+UV aging experiments.

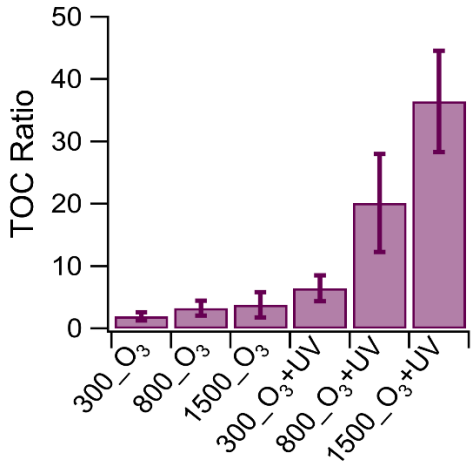

Figure S16. The total organic content (TOC) ratios of aged to fresh particles extract.

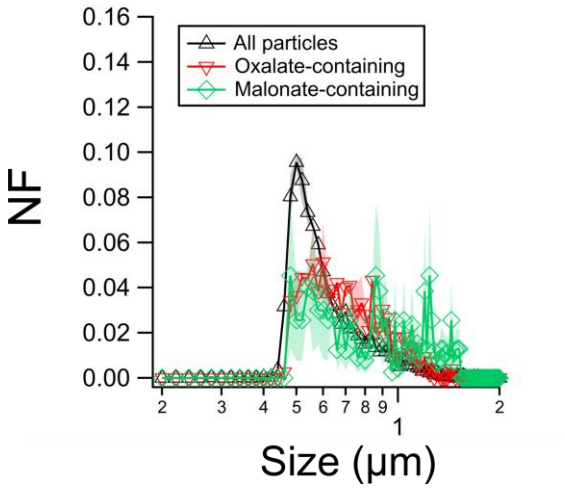

Figure S17. Size distribution (0.2-2 μm) of O_3-UV-aged particles (at 1500 ppb O_3 and UV) and their dicarboxylate-containing fractions. The shadings show one standard deviation.

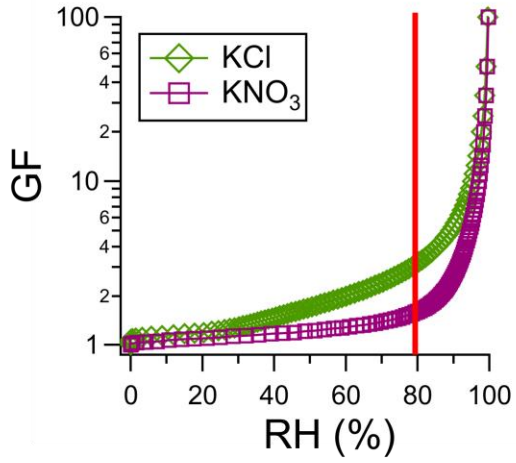

Figure S18. The GF of KCl and KNO_3 particles as a function of RH. The red line denotes 80% RH.

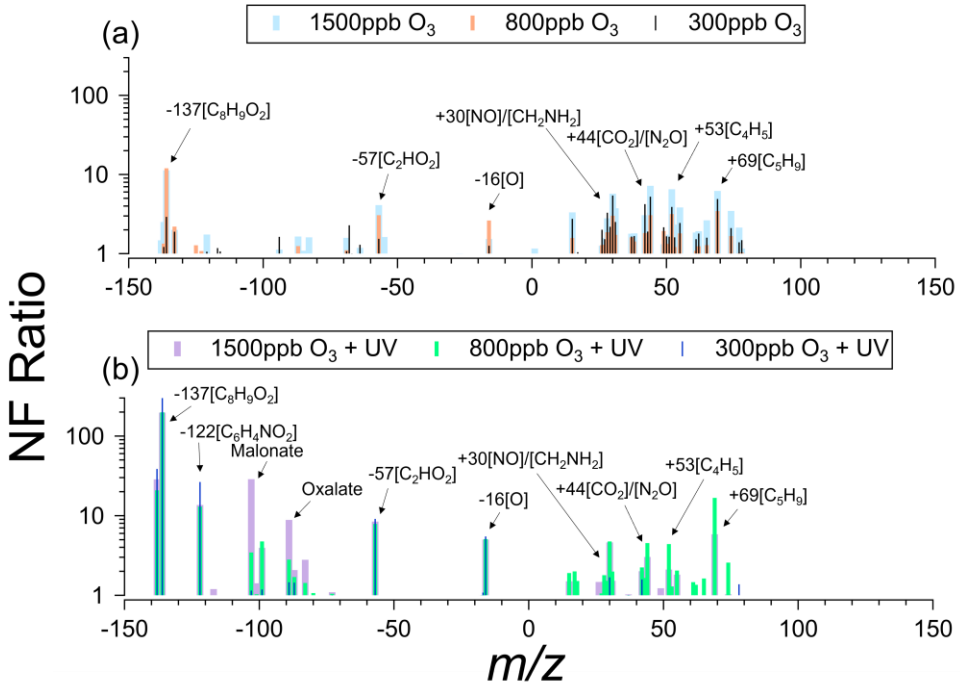

Figure S19. The NF ratio (aged to fresh) of (a) O_3-Dark-aged, (b) O_3-UV-aged particles to fresh particles, as a function of m/z [-150, 150].

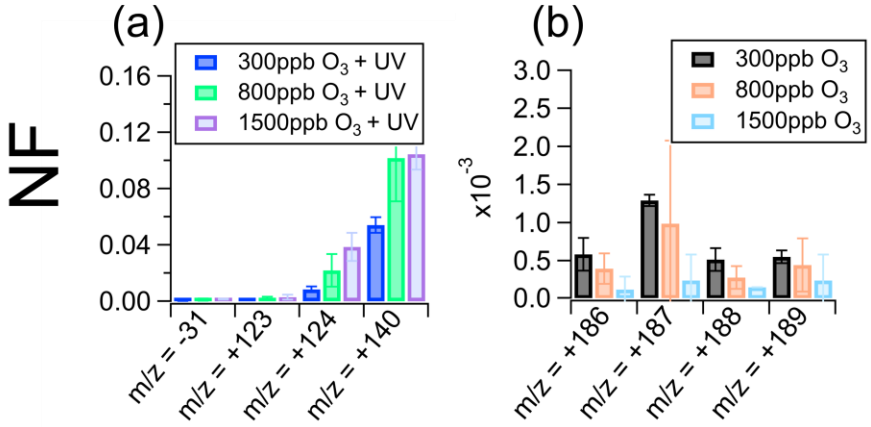

Figure S20. The NF of new organic peaks in aged particles.

Table S1. The classification of particles and RPA of total nitrate peaks of aged particles at different laser fluences.

Experimental Conditions	Laser fluence (mJ)	OC-ON (%)	OC-N (%)	K-ON (%)	K-ONN (%)	K-N (%)	K-ONEC (%)	K-Cl (%)	$RPA_{Total\ nitrate}$
O_3-dark-aged (800 ppb)	0.6	(7.6±1.0)	(21.9±1.7)	(29.0±0.7)	(11.2±0.9)	(2.5±0.5)	(22.8±1.8)	(3.9±0.4)	(0.40±0.15)
	1.2	(7.2±1.4)	(22.6±4.0)	(28.5±4.3)	(10.6±0.2)	(3.3±1.3)	(22.8±2.5)	(4.0±0.1)	(0.37±0.09)
O_3-UV-aged (800 ppb)	0.6	(0.0±0.0)	(36.7±7.2)	(0.0±0.0)	(26.7±2.1)	(35.5±4.2)	(0.0±0.0)	(0.0±0.0)	(0.66±0.03)
	1.2	(0.0±0.0)	(35.6±2.3)	(0.0±1.0)	(28.6±1.9)	(33.6±4.7)	(0.2±0.2)	(0.0±0.0)	(0.67±0.07)

Table S2. Potential peaks from the inorganics and elemental carbons.

	m/z	Formula	Ref
Inorganic salts	-163	KNO_3	(Pratt et al., 2011)
	-155	Na_2Cl_3	(Harrison et al., 2012)
	-153		
	-151		
	-147	$Na(NO_3)_2$	(Ault et al., 2014)
	-131	$NaNO_3NO_2$	(Ault et al., 2014)
	-125	$H(NO_3)_2$	
	-113	KCl_2	(Bi et al., 2011)
	-111		
	-109		
	-101	$KNO_3/NaNONO_2$	(Ault et al., 2014)
	-97	$HSO_4/NaCl_2$	(Liang et al., 2022)
	-96	SO_4	
	-95	$NaCl_2$	(Ault et al., 2014)
	-93		
	-62	NO_3	(Cheng et al., 2017)
	-58	NaCl	(Zhu et al., 2020)
	-46	NO_2	(Cheng et al., 2017)
	-37	Cl	(Ault et al., 2014)
	-35		
	+23	Na	(Dall'osto et al., 2004)
	+39	K	(Bi et al., 2011)
	+41		
	+63	Na_2OH	(Yang et al., 2009)
	+81	Na_2Cl	(Dall'osto et al., 2004)
	+83		
	+97	NaKCl	(Gross et al., 2000)
	+113	K_2Cl	(Silva et al., 1999)
	+115		

	+139 +141	Na_3Cl_2	(Dall'osto et al., 2004)
Elemental carbons	±12n	C_n	(Zhou et al., 2022)

Reference

Ault, A. P., Guasco, T. L., Baltrusaitis, J., Ryder, O. S., Trueblood, J. V., Collins, D. B., Ruppel, M. J., Cuadra-Rodriguez, L. A., Prather, K. A., and Grassian, V. H.: Heterogeneous Reactivity of Nitric Acid with Nascent Sea Spray Aerosol: Large Differences Observed between and within Individual Particles, The Journal of Physical Chemistry Letters, 5, 2493-2500, 10.1021/jz5008802, 2014.

Bi, X., Zhang, G., Li, L., Wang, X., Li, M., Sheng, G., Fu, J., and Zhou, Z.: Mixing state of biomass burning particles by single particle aerosol mass spectrometer in the urban area of PRD, China, Atmospheric Environment, 45, 3447-3453, https://doi.org/10.1016/j.atmosenv.2011.03.034, 2011.

Cheng, C., Li, M., Chan, C. K., Tong, H., Chen, C., Chen, D., Wu, D., Li, L., Wu, C., and Cheng, P.: Mixing state of oxalic acid containing particles in the rural area of Pearl River Delta, China: implications for the formation mechanism of oxalic acid, Atmospheric Chemistry and Physics, 17, 9519-9533, 2017.

Dall'Osto, M., Harrison, R. M., Coe, H., and Williams, P.: Real-time secondary aerosol formation during a fog event in London, Atmos. Chem. Phys., 9, 2459-2469, 10.5194/acp-9-2459-2009, 2009.

Dall'Osto, M., Beddows, D. C. S., Kinnersley, R. P., Harrison, R. M., Donovan, R. J., and Heal, M. R.: Characterization of individual airborne particles by using aerosol time-of-flight mass spectrometry at Mace Head, Ireland, Journal of Geophysical Research: Atmospheres, 109, https://doi.org/10.1029/2004JD004747, 2004.

Dall'Osto, M., Ovadnevaite, J., Ceburnis, D., Martin, D., Healy, R. M., O'Connor, I. P., Kourtchev, I., Sodeau, J. R., Wenger, J. C., and O'Dowd, C.: Characterization of urban aerosol in Cork city (Ireland) using aerosol mass spectrometry, Atmospheric Chemistry and Physics, 13, 4997-5015, 2013.

Davis, D., Ravishankara, A., and Fischer, S.: SO2 oxidation via the hydroxyl radical: atmospheric fate of HSOx radicals, Geophysical Research Letters, 6, 113-116, 1979.

Diab, J., Streibel, T., Cavalli, F., Lee, S., Saathoff, H., Mamakos, A., Chow, J., Chen, L.-W., Watson, J., and Sippula, O.: Hyphenation of a EC/OC thermal–optical carbon analyzer to photo-ionization time-of-flight mass spectrometry: an off-line aerosol mass spectrometric approach for characterization of primary and secondary particulate matter, Atmospheric Measurement Techniques, 8, 3337-3353, 2015.

Gaie-Levrel, F., Perrier, S., Perraudin, E., Stoll, C., Grand, N., and Schwell, M.: Development and characterization of a single particle laser ablation mass spectrometer (SPLAM) for organic aerosol studies, Atmospheric Measurement Techniques, 5, 225-241, 2012.

Gross, D. S., Gälli, M. E., Silva, P. J., and Prather, K. A.: Relative sensitivity factors for alkali metal and ammonium cations in single-particle aerosol time-of-flight mass spectra, Analytical Chemistry, 72, 416-422, 2000.

Harrison, R. M., Dall'Osto, M., Beddows, D., Thorpe, A. J., Bloss, W. J., Allan, J. D., Coe, H., Dorsey, J. R., Gallagher, M., and Martin, C.: Atmospheric chemistry and physics in the atmosphere of a developed megacity (London): an overview of the REPARTEE experiment and its conclusions, Atmospheric Chemistry and Physics, 12, 3065-3114, 2012.

Liang, Z., Zhou, L., Infante Cuevas, R. A., Li, X., Cheng, C., Li, M., Tang, R., Zhang, R., Lee, P. K. H., Lai, A. C. K., and Chan, C. K.: Sulfate Formation in Incense Burning Particles: A Single-Particle Mass Spectrometric Study, Environmental Science & Technology Letters, 10.1021/acs.estlett.2c00492, 2022.

Pagels, J., Dutcher, D. D., Stolzenburg, M. R., McMurry, P. H., Gälli, M. E., and Gross, D. S.: Fine-particle emissions from solid biofuel combustion studied with single-particle mass spectrometry: Identification of markers for organics, soot, and ash components, Journal of Geophysical Research: Atmospheres, 118, 859-870, https://doi.org/10.1029/2012JD018389, 2013.

Pratt, K., Murphy, S., Subramanian, R., DeMott, P., Kok, G., Campos, T., Rogers, D., Prenni, A., Heymsfield, A., and Seinfeld, J.: Flight-based chemical characterization of biomass burning aerosols within two prescribed burn smoke plumes, Atmospheric Chemistry and Physics, 11, 12549-12565, 2011.

Qin, X. and Prather, K. A.: Impact of biomass emissions on particle chemistry during the California Regional Particulate Air Quality Study, International Journal of Mass Spectrometry, 258, 142-150, https://doi.org/10.1016/j.ijms.2006.09.004, 2006.

Silva, P. J. and Prather, K. A.: Interpretation of mass spectra from organic compounds in aerosol time-of-flight mass spectrometry, Analytical Chemistry, 72, 3553-3562, 2000.

Silva, P. J., Liu, D.-Y., Noble, C. A., and Prather, K. A.: Size and Chemical Characterization of Individual Particles Resulting from Biomass Burning of Local Southern California Species, Environmental Science & Technology, 33, 3068-3076, 10.1021/es980544p, 1999.

Sullivan, R. C. and Prather, K. A.: Investigations of the diurnal cycle and mixing state of oxalic acid in individual particles in Asian aerosol outflow, Environmental Science Technology, 41, 8062-8069, 2007.

Wang, X., Zhang, Y., Chen, H., Yang, X., Chen, J., and Geng, F.: Particulate nitrate formation in a highly polluted urban area: a case study by single-particle mass spectrometry in Shanghai, Environmental Science & Technology, 43, 3061-3066, 2009.

Yang, F., Chen, H., Wang, X., Yang, X., Du, J., and Chen, J.: Single particle mass spectrometry of oxalic acid in ambient aerosols in Shanghai: Mixing state and formation mechanism, Atmospheric Environment, 43, 3876-3882, 2009.

Zhou, L., Li, M., Cheng, C., Zhou, Z., Nian, H., Tang, R., and Chan, C. K.: Real-time chemical characterization of single ambient particles at a port city in Chinese domestic emission control area — Impacts of ship emissions on urban air quality, Science of The Total Environment, 819, 153117, https://doi.org/10.1016/j.scitotenv.2022.153117, 2022.

Zhu, S., Li, L., Wang, S., Li, M., Liu, Y., Lu, X., Chen, H., Wang, L., Chen, J., and Zhou, Z.: Development of an automatic linear calibration method for high-resolution single-particle mass spectrometry: improved chemical species identification for atmospheric aerosols, Atmospheric Measurement Techniques, 13, 4111-4121, 2020.

Zuend, A., Marcolli, C., Luo, B. P., and Peter, T.: A thermodynamic model of mixed organic-inorganic aerosols to predict activity coefficients, Atmos. Chem. Phys., 8, 4559-4593, 10.5194/acp-8-4559-2008, 2008.